Chapter 7

An unsteady analytical model for the complete lifecycle of dust devils from genesis to decay

A dust devil is a tiny, rotating column of air that forms over hot, dry surfaces and is identified by a visible swirl of dirt, dust, and debris that has been lifted from the ground. They may ascend from a few feet to several hundred feet, and last a few minutes, but can sometimes last longer. Dust devils are commonly observed in desert areas on Earth and have also been reported on Mars Fernández (1997); Greeley et al. (2003); Fisher et al. (2005); Balme and Greeley (2006a); Reiss et al. (2014). Dust devil studies reveal their formation, evolution, and environmental impact, while modelling attempts aim to replicate the processes underlying their initiation, growth, and ultimate weakening.

The contents of this chapter have been communicated in **Journal of Fluid Mechanics** for the publication.

Early field measurements by Sinclair (1966) in Arizona measured the key physical characteristics such as diameter, height, wind speeds (up to 20–25 m/s), and temperature anomalies—linking dust devil formation to solar heating and convective instability. Subsequent studies expanded this empirical foundation. Farrell et al. (2003c) gave an electrodynamic model, illustrates the particle collisions within the vortex generate charge separation and strong electric fields, producing a dipole-like structure consistent with observations. Bluestein et al. (2004) incorporated Doppler radar to measure wind velocities (up to 25–30 m/s) in Texas, correlating dust devil intensity, size, and lifespan with surface heating and wind shear.

Developments in experimental and numerical methods have improved our comprehension even more. Kanak (2005) examined the initiation and evolution of dust devils under idealised conditions using high-resolution simulations, emphasising the crucial roles of boundary layer characteristics, wind shear, and surface heating. The impact of surface roughness was investigated in laboratory experiments by Neakrase and Greeley (2010). They focused on the ideal roughness ($\lambda \approx 0.01$–0.1) that increases sediment lifting by lowering threshold velocities for fine particles ($< 100\,\mu$m), while excessive roughness ($\lambda \approx 0.11$–0.23) dissipates energy and decreases tangential velocities. Horton et al. (2016) combined modelling, simulations, and experiments, emphasising the role of vorticity and thermal convection in particle entrainment and vortex formation.

Despite these developments, inviscid, time-independent models have been used in many atmospheric vortex studies to describe steady-state dynamics. Although these methods offer important insights into the structure of vortices, they are unable to capture the dust devils' fleeting lifecycle. A steady-state parametric wind profile, developed by Wood and White (2011) gave a steady-state parametric wind profile that predicts velocity decay without taking viscosity or temporal evolution into consideration. Similarly, hurricane-like vortices with a stable, inviscid core-annulus structure are modelled

by Nolan et al. (2001). Exact solutions for annular vortex flows under time-independent assumptions were derived by Pandey and Maurya (2018b). Other models, such as those by Sohn (2020) and Baker and Sterling (2017), employed potential flow frameworks and steady inviscid base flows. An analytical model for tornado-like vortices based on force balance under the assumption of a steady-state structure was presented by Zhang et al. (2023). These models are useful for characterising equilibrium states, but they fail to account for the quick formation, maturation, and decay of natural dust devils, where temporal dynamics and viscous dissipation play a critical role.

Attempts to address the time evolution of dust devils remain limited. Onishchenko et al. (2015) proposed an unsteady model based on convective cell dynamics, deriving a stream function that speculates rapid vorticity growth in an unstably stratified atmosphere. Their formulation permits indefinite growth with time and axial extent, which is not as unrealistic as real dust devils weaken and dissipate. Meanwhile, Sheel et al. (2021) studied steady-state dust lifting but did not incorporate time-dependent dynamics. These limitations highlight the need for dynamic, time-dependent models that more accurately illustrate the transient nature of dust devils.

The objectives of this study is to fill these gaps by developing a time-dependent viscous model that depicts the entire lifecycle of dust devils, from their quick formation to their slow decay. Dust devils have been observed to form in a matter of seconds, mature quickly, and last for a few minutes before fading away. Moreover, the axial and radial velocities decrease with maturity, but azimuthal rotation keeps the vortex going until environmental conditions cause it to disintegrate.

In this work, a mathematical formulation incorporating temporal evolution is presented. The model provides a thorough understanding of dust devils' entire lifecycle and impacts by bridging the gap between steady-state assumptions and observed dynamics by taking into account both viscous and transient effects.

7.1 Mathematical formulation of the problem

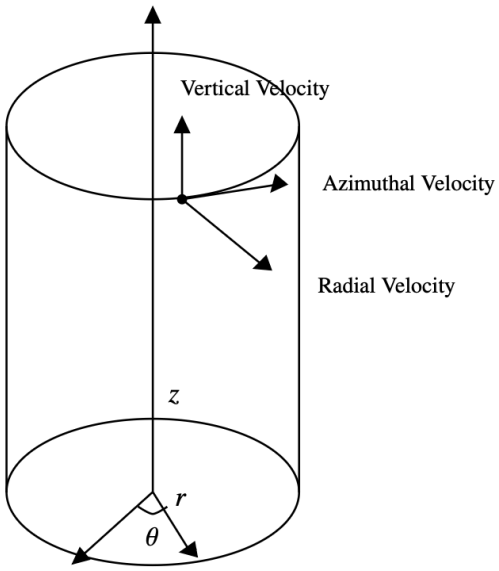

Figure 7.1: Cylindrical coordinate system for Dust devils

The unsteady axi-symmetric flow of incompressible, Newtonian, viscous fluids is described in cylindrical polar coordinates ($\tilde{r}$, $\tilde{\theta}$, $\tilde{z}$), as shown in Fig. (7.1), by Navier-Stokes equations along with the continuity equation as

$$\frac{1}{\tilde{r}}\frac{\partial(\tilde{r}\tilde{u})}{\partial\tilde{r}} + \frac{\partial\tilde{w}}{\partial\tilde{z}} = 0, \tag{7.1}$$

$$\left(\frac{\partial\tilde{u}}{\partial\tilde{t}} + \tilde{u}\frac{\partial\tilde{u}}{\partial\tilde{r}} + \tilde{w}\frac{\partial\tilde{u}}{\partial\tilde{z}} - \frac{\tilde{v}^2}{\tilde{r}}\right) = -\frac{1}{\rho}\frac{\partial\tilde{p}}{\partial\tilde{r}} + \nu\left(\frac{\partial^2\tilde{u}}{\partial\tilde{r}^2} + \frac{1}{\tilde{r}}\frac{\partial\tilde{u}}{\partial\tilde{r}} - \frac{\tilde{u}}{\tilde{r}^2} + \frac{\partial^2\tilde{u}}{\partial\tilde{z}^2}\right), \tag{7.2}$$

$$\left(\frac{\partial\tilde{v}}{\partial\tilde{t}} + \tilde{u}\frac{\partial\tilde{v}}{\partial\tilde{r}} + \tilde{w}\frac{\partial\tilde{v}}{\partial\tilde{z}} + \frac{\tilde{u}\tilde{v}}{\tilde{r}}\right) = \nu\left(\frac{\partial^2\tilde{v}}{\partial\tilde{r}^2} + \frac{1}{\tilde{r}}\frac{\partial\tilde{v}}{\partial\tilde{r}} - \frac{\tilde{v}}{\tilde{r}^2} + \frac{\partial^2\tilde{v}}{\partial\tilde{z}^2}\right), \tag{7.3}$$

$$\left(\frac{\partial\tilde{w}}{\partial\tilde{t}} + \tilde{u}\frac{\partial\tilde{w}}{\partial\tilde{r}} + \tilde{w}\frac{\partial\tilde{w}}{\partial\tilde{z}}\right) = -\frac{1}{\rho}\frac{\partial\tilde{p}}{\partial\tilde{z}} + \tilde{F}_z + \nu\left(\frac{\partial^2\tilde{w}}{\partial\tilde{r}^2} + \frac{1}{\tilde{r}}\frac{\partial\tilde{w}}{\partial\tilde{r}} + \frac{\partial^2\tilde{w}}{\partial\tilde{z}^2}\right), \tag{7.4}$$

Here $\tilde{u}$, $\tilde{v}$, $\tilde{w}$ denote the radial, azimuthal, axial components of velocity while $\tilde{t}$ is time, $\tilde{p}$ pressure, $\tilde{F}_z = g(\rho - \rho_\infty)/\rho_\infty$ buoyancy, g the gravitational acceleration, ρ, ρ_∞ the

densities of the vortex and the ambient wind respectively, and ν the kinematic viscosity of the fluid. To achieve dynamical similarity, we transform the governing equations (1-4) into a non-dimensional form by introducing the following dimensionless variables:

$$r = \frac{\tilde{r}}{r_m}, z = \frac{\tilde{z}}{r_m}, t = \frac{\tilde{t}v_m}{r_m}, u = \frac{\tilde{u}}{v_m}, v = \frac{\tilde{v}}{v_m}, w = \frac{\tilde{w}}{v_m}, p = \frac{\tilde{p}}{\rho v_m^2}, F = \frac{\tilde{F}_z}{v_m^2/r_m}, \quad (7.5)$$

r_m being the characteristics radius where the azimuthal velocity is maximum, v_m the maximum azimuthal velocity at the radius $\tilde{r} = r_m$, $\tilde{z} = 0$ and $\tilde{t} = r_m/v_m$. This is worth noting that the maximum azimuthal velocity is however dependent on $\tilde{z}$.

Using (7.5), equations (7.1) - (7.4) transform to

$$\frac{\partial u}{\partial t} + u\frac{\partial u}{\partial r} + w\frac{\partial u}{\partial z} - \frac{v^2}{r} = -\frac{\partial p}{\partial r} + \frac{1}{Re}\left(\frac{\partial^2 u}{\partial r^2} + \frac{1}{r}\frac{\partial u}{\partial r} + \frac{\partial^2 u}{\partial z^2} - \frac{u}{r^2}\right), \quad (7.6)$$

$$\frac{\partial v}{\partial t} + u\frac{\partial v}{\partial r} + w\frac{\partial v}{\partial z} + \frac{uv}{r} = \frac{1}{Re}\left(\frac{\partial^2 v}{\partial r^2} + \frac{1}{r}\frac{\partial v}{\partial r} + \frac{\partial^2 v}{\partial z^2} - \frac{v}{r^2}\right), \quad (7.7)$$

$$\frac{\partial w}{\partial t} + u\frac{\partial w}{\partial r} + w\frac{\partial w}{\partial z} = -\frac{\partial p}{\partial z} + F + \frac{1}{Re}\left(\frac{\partial^2 w}{\partial r^2} + \frac{1}{r}\frac{\partial w}{\partial r} + \frac{\partial^2 w}{\partial z^2}\right), \quad (7.8)$$

$$\frac{1}{r}\frac{\partial}{\partial r}(ru) + \frac{\partial w}{\partial z} = 0, \quad (7.9)$$

where $Re = v_m r_m/\nu$ denotes the Reynolds number and $F = \tilde{F}_z/(v_m^2/r_m)$, the body force.

7.2 Analysis

In modelling the temporal evolution of dust devils, we assume that their characteristic strength first rapidly intensifies and subsequently decays over time. A simple logistic-type ordinary differential equation,

$$\frac{d\Gamma}{dt} = a\Gamma - b\Gamma^2,$$

captures this behaviour, exhibiting initial exponential growth followed by saturation and decay. To reflect this physical process while maintaining mathematical tractability, we model the time dependence as

$$\exp\left(-\lambda\frac{t^2+1}{t}\right),$$

where λ is a positive parameter. For small t, the $1/t$ term suppresses premature growth; around $t \sim 1$, the strength peaks; and for large t, the system decays exponentially, consistent with observed dust devil lifecycles.

This model builds upon the hydrodynamic framework of Onishchenko et al. (2015), who split the velocity field into poloidal and toroidal parts. Assuming radial derivatives dominate over axial ones, they derived a stream function for an unsteady, axisymmetric flow

$$\psi = \frac{ar^2z}{2}e^{\left(\lambda t-\frac{r^2}{r_m^2}\right)},$$

where λ is a growth parameter, a is a constant, and r_m is the characteristic core radius. However, their formulation predicts continuous, indefinite growth of the axial velocity for positive λ, an unrealistic outcome for natural vortices that weaken and dissipate over time.

To address the limitations of previous models and describe the full lifecycle of a dust devil, we propose a modified stream function in dimensionless form

$$\psi = Ar^2ze^{-\lambda\left(\frac{t^2+1}{t}\right)-r^2}, \tag{7.10}$$

where A is a constant. Although the flow is three-dimensional, the Stokes stream function remains feasible, and the velocity components are derived as

$$u = -\frac{1}{r}\frac{\partial\psi}{\partial z}, \qquad w = \frac{1}{r}\frac{\partial\psi}{\partial r}. \tag{7.11}$$

Substituting stream-function into Eq. (7.11) yields

$$u(r,t) = -Are^{-\lambda\left(\frac{t^2+1}{t}\right)-r^2}, \tag{7.12}$$

$$w(r,z,t) = 2Az(1-r^2)e^{-\lambda\left(\frac{t^2+1}{t}\right)-r^2}. \tag{7.13}$$

It is readily verified that the initial condition $u(r,0) = 0$ is satisfied.

To determine A, we observe that the maximum (in magnitude) of the radial velocity u occurs at $r = 1/\sqrt{2}$ and $t = 1$, we yield

$$A = -u_m e^{2\lambda}\sqrt{2e}, \tag{7.14}$$

where u_m is the magnitude of the maximum radial velocity. Substituting u and w into the radial and axial momentum equations, we obtain the pressure gradients

$$\begin{aligned}\frac{v^2}{r} - \frac{\partial p}{\partial r} = {} & A\lambda r\left(\frac{t^2-1}{t^2}\right)e^{-\lambda\left(\frac{t^2+1}{t}\right)-r^2} + A^2(r-2r^3)e^{-2\left(\lambda\left(\frac{t^2+1}{t}\right)+r^2\right)} \\ & - \frac{A}{Re}(8r-4r^3)e^{-\lambda\left(\frac{t^2+1}{t}\right)-r^2},\end{aligned} \tag{7.15}$$

and

$$\begin{aligned}\frac{\partial p}{\partial z} = {} & \frac{2Az}{Re}(-4r^4+16r^2-8)e^{-\lambda\left(\frac{t^2+1}{t}\right)-r^2} \\ & + 2A\lambda z(1-r^2)\left(\frac{t^2-1}{t^2}\right)e^{-\lambda\left(\frac{t^2+1}{t}\right)-r^2} \\ & - 4A^2ze^{-2\left(\lambda\left(\frac{t^2+1}{t}\right)+r^2\right)}.\end{aligned} \tag{7.16}$$

Integrating Eq. (7.16) with respect to z yields the pressure

$$\begin{aligned} p(r,z,t) = \frac{Az^2}{Re}(-4r^4+16r^2-8)e^{-\lambda\left(\frac{t^2+1}{t}\right)-r^2} \\ + A\lambda z^2(1-r^2)\left(\frac{1-t^2}{t^2}\right)e^{-\lambda\left(\frac{t^2+1}{t}\right)-r^2} \\ - 2A^2z^2e^{-2\left(\lambda\left(\frac{t^2+1}{t}\right)+r^2\right)} + f(r,t), \end{aligned} \tag{7.17}$$

where $f(r,t)$ is an arbitrary function of r and t. Differentiating Eq. (7.17) with respect to r yields

$$\begin{aligned} \frac{\partial p}{\partial r} = \frac{4Az^2}{Re}(2r^5-12r^3+12r)e^{-\lambda\left(\frac{t^2+1}{t}\right)-r^2} \\ + A\lambda z^2(2r^3-4r)\left(\frac{t^2-1}{t^2}\right)e^{-\lambda\left(\frac{t^2+1}{t}\right)-r^2} \\ + 8A^2z^2re^{-2\left(\lambda\left(\frac{t^2+1}{t}\right)+r^2\right)} + \frac{\partial f}{\partial r}. \end{aligned} \tag{7.18}$$

The azimuthal velocity v can now be expressed as

$$\begin{aligned} v = \Bigg[\frac{4r^2A}{Re}\Big\{2z^2(r^4-6r^2+6)+(r^2-2)\Big\}e^{-\lambda\left(\frac{t^2+1}{t}\right)-r^2} \\ + r^2A^2\Big\{(1-2r^2)+8z^2\Big\}e^{-2\left(\lambda\left(\frac{t^2+1}{t}\right)+r^2\right)} \\ + A\lambda r^2\Big\{1+2z^2(r^2-2)\Big\}\left(\frac{t^2-1}{t^2}\right)e^{-\lambda\left(\frac{t^2+1}{t}\right)-r^2} + r\eta(r)e^{-\lambda\left(\frac{t^2+1}{t}\right)-r^2}\Bigg]^{1/2}, \end{aligned} \tag{7.19}$$

where we assume $f'(r,t) = \eta(r)e^{-\lambda\left(\frac{t^2+1}{t}\right)-r^2}$ and $\eta(r) = Br$. Applying the boundary condition $v = 1$ at $z = 0$, $r = 1$, $t = 1$, the constant B is determined as

$$B = e^{2\lambda+1} + \frac{4A}{Re} + A^2e^{-2\lambda-1}. \tag{7.20}$$

Finally, the pressure field is obtained as

$$
\begin{aligned}
p(r,z,t) = \frac{Az^2}{Re}(-4r^4+16r^2-8)e^{-\lambda\left(\frac{t^2+1}{t}\right)-r^2} \\
- A\lambda z^2(1-r^2)\left(\frac{1-t^2}{t^2}\right)e^{-\lambda\left(\frac{t^2+1}{t}\right)-r^2} \\
- 2A^2z^2e^{-2\left(\lambda\left(\frac{t^2+1}{t}\right)+r^2\right)} - \frac{1}{2}\left(e^{2\lambda+1}+\frac{4A}{Re}+A^2e^{-2\lambda-1}\right)e^{-\lambda\left(\frac{t^2+1}{t}\right)-r^2}.
\end{aligned}
\tag{7.21}
$$

Typical dust devils exhibit core radii of 5–50 m, peak azimuthal velocities of 5–30 m/s, and heights ranging from 10–1000 m (Sinclair (1966); Greeley et al. (2003); Bluestein et al. (2004)). These imply Reynolds numbers $Re \sim 10^6$–10^7, characteristic of highly turbulent flows. For this study, we adopt $r_m = 10$ m and $v_m = 10$ m/s, yielding $Re \sim 6.67 \times 10^6$. For comparison, moderate values ($Re = 1000$–5000) are also explored. A characteristic decay time of 200 s gives a dimensionless decay rate $\lambda \sim 0.0125$, ensuring realistic temporal evolution.

7.3 Results and Discussion

7.3.1 Radial Velocity

The derived radial velocity Eq. (7.12) attains the maximum magnitude when $r = 1/\sqrt{2}$ and $t = 1$ (see Appendix). For this reason, we analyse it by plotting diagrams of the radial profiles for the time intervals [0,1] and $t \geq 1$, respectively, in Fig. (7.2) and Fig. (7.3). The plots precisely demonstrate dust devil formation, growth, and decay. The detailed illustrations follow.

Fig. (7.2) demonstrates the development phase of the dust devil. During this phase, radial wind becomes increasingly prominent over a short period, strengthening the

vortex's motion (the facts will be clearer when we discuss rotational motion in subsection 7.3.3). Initially, the dust devil forms when the radial wind moves from a large distance (theoretically from infinity) toward the low-pressure centre to fill the void region. As time progresses within this interval, the radial velocity increases towards the centre, indicating intensification of the dust devil, and reaches the maximum at $r = 1/\sqrt{2}$. Beyond this peak, the velocity declines and eventually vanishes at the centre of the vortex. This trend demonstrates that during the initial stages ($t \in [0, 1]$), the dust devil intensifies, with its radial velocity actively growing and propagating inward.

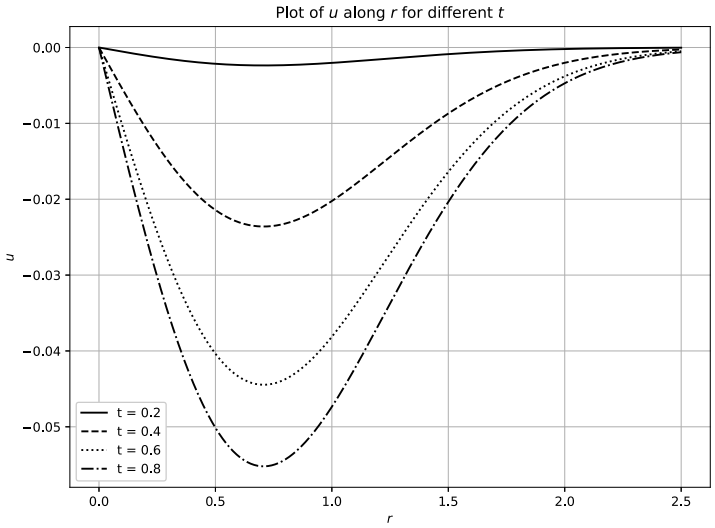

Figure 7.2: The plot presents the radial profiles of normalized radial velocities for time range $0 - 1$ for $z = 1$, $\lambda = 1$ and $A = 1$. Negative values of u simply indicate that the radial velocity is directed towards the axis.

Fig. (7.3) shows contrasting behaviour observed during the decay phase. Plots reveal that the magnitude of radial velocity lessens with time beyond $t = 1$ and finally reduces to zero for very large values, indicating the disappearance of the vortex eventually. This is also confirmed by the theoretical model of u, which tends to zero as $t \to \infty$. This span of time from $t = 1$ onwards displays decaying of the dust devils consuming a larger interval of time, which was formed almost transiently during t varying from $0 - 1$. This

resembles the process of natural occurrence of dust devils. Another graph, viz. Fig. (7.4), which has radial velocity plotted against time corresponding to $r = 1 - 3$, reveals that the dust devils have a finite size as the velocity diminishes drastically for values higher than $r = 1$.

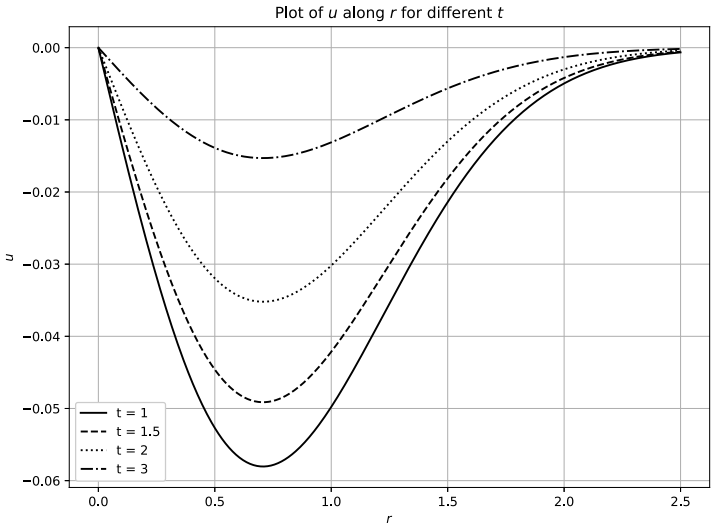

Figure 7.3: The plot presents the radial profiles of normalized radial velocities for time range $1 - 2$ for $z = 1$, $\lambda = 1$ and $A = 1$. Negative values of u simply indicate that the radial velocity is directed towards the axis.

These observations depict the transition from an intensifying phase to a decaying phase, capturing the complete temporal evolution of the radial velocity in a dust devil. The overall magnitude of the velocity is smaller during the decay phase, indicating a weakening dust devil structure. This phase marks the decay of the dust devil, with diminishing radial motion.

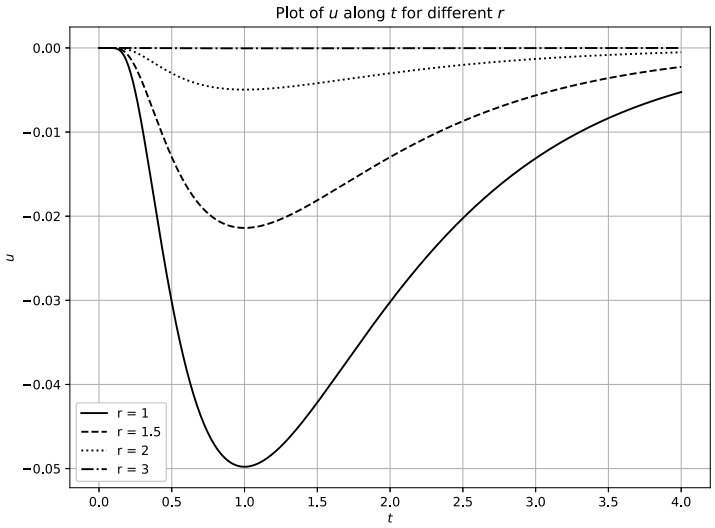

Figure 7.4: The plot presents the profiles of normalized radial velocities along time for radii $1-3$ for $z=1$, $\lambda=1$ and $A=1$. Negative values of u simply indicate that the radial velocity is directed towards the axis.

7.3.2 Axial Velocity

The two figures (Fig. 7.5, 7.6) illustrate the evolution of the normalized axial velocity along the radial direction at different time intervals, capturing the formation, intensification, and eventual decay of dust devils. In Fig. (7.5), corresponding to the time interval $0 \leq t \leq 1$, the axial velocity is maximum near the centre and gradually decreases outward. As time progresses ($t = 0-1$), the peak velocity increases, indicating thereby that the strong updrafts are concentrated at the centre. Increasing peak velocity marks the strengthening of vertical motion. While axial velocity increases in the range $t = 0-1$, it is observed to decrease in the range $t = 1-4$, although not shown, it continues to decrease with time even beyond the given range. A slowing down of velocity indicates that the dust devil is weakening. This phase corresponds to the dissipation stage, where the vortex loses its intensity, and velocity diminishes over time. The temporal evolution of axial velocity in a dust devil, transitioning from a phase of strengthening upward motion

($t \in [0, 1]$) to one of gradual weakening and dissipation ($t \in [1, 4]$) indicate that a dust devil forms almost instantaneously i.e., it scales its full height in a very short period but takes time to decay, which is much slower.

At the vortex centre, axial velocity is maximum, while radial velocity is zero, a characteristic of vortices driven by low-pressure updrafts (Fig. 7.3, 7.5). Over time both the velocity components strengthen during intensification (during $t = 0 - 1$) and weaken as the dust devil dissipates (during $t \geq 1$).

Fig. (7.7) illustrates the temporal evolution of the normalized axial velocity at different radial positions ($r = 0 - 1$) within the dust devil. Initially, during ($0 \leq t \leq 1$), axial velocity increases across all radii, with the strongest updraft occurring near the vortex centre. This pattern is consistent with the dust devil dynamics, which are driven vertically by a central low-pressure area and maintained by radial inflow. As the dust devil evolves, axial velocity reaches its peak at $t \approx 1$. In the dissipation phase ($t > 1$), axial velocity declines, with the decay rate being significant at larger radii, indicating that the outer regions lose convective strength earlier than the centre. According to this pattern, the dust devil has a structured life cycle, with peak intensity concentrated in the centre and a weakening process that spreads outward until the vortex dissipates.

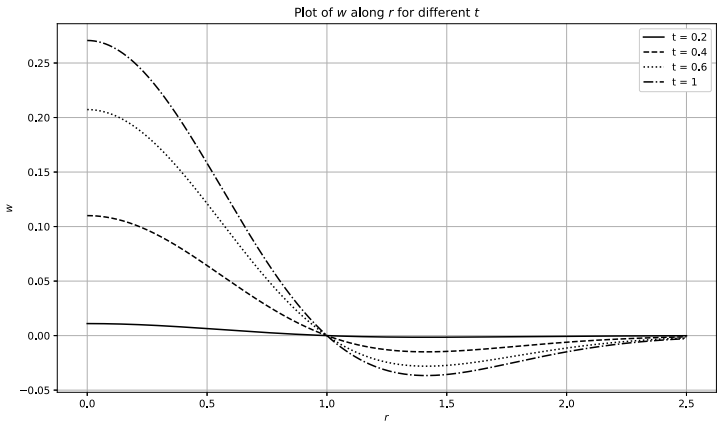

Figure 7.5: The plot presents the radial profiles of normalized axial velocities for time range $0 - 1$ for $z = 1$, $\lambda = 1$ and $A = 1$.

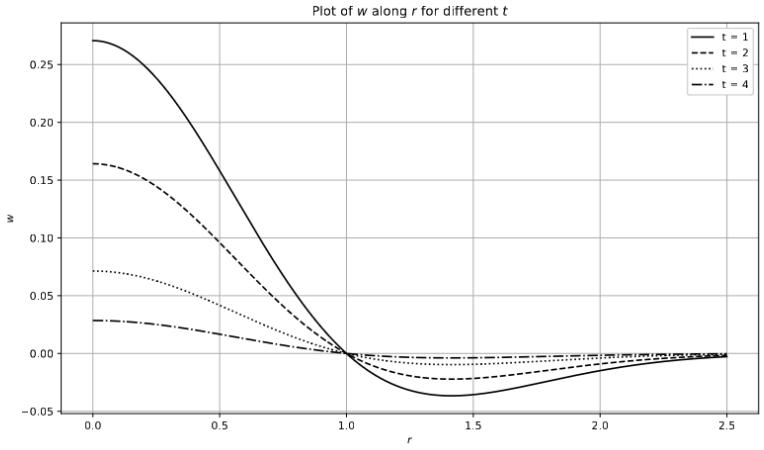

Figure 7.6: The plot presents the radial profiles of normalized axial velocities for time range $1-4$ for $z=1$, $\lambda=1$ and $A=1$.

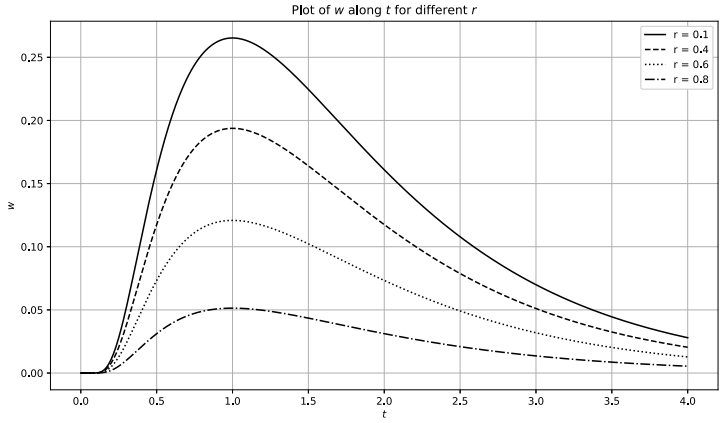

Figure 7.7: The plot presents the profiles of normalized axial velocities along time for radius in the range $0-1$ for $z=1$, $\lambda=1$ and $A=1$.

7.3.3 Azimuthal Velocity

The radial profiles of azimuthal velocity at durations $t \in [0,1]$ (Fig. 7.8) and $t \in [1,3]$ (Fig. 7.9) illustrate the evolution of rotational motion. At the vortex centre, the azimuthal velocity is zero. It rises with radius, reaching the peak at $r = 1$. Beyond this peak, it begins to fall, but at a slower rate, to eventually vanish somewhere along the radius. This behaviour indicates that the rotational motion dominates around the low-pressure region.

The increasing trend of velocity with time indicates the intensification of the dust devil. During $t \in [0, 1]$, wind rotation is observed to intensify with time, rising to the maximum at $t = 1$. This takes place in a very short span of time. While contrary to that, the duration ($t \in [1, 4]$) exhibits the opposite trend. The peak azimuthal velocity starts to fall with time beyond $t = 1$, rather slowly, indicating the weakening of the rotational velocity. This is the most interesting observation that the formation of the dust devil, together with intensification, takes place almost instantaneously, while its decay spans over a much longer duration. This is the exact resemblance to the naturally occurring dust devils. Fig. (7.10) and (7.11) illustrate the temporal evolution of normalized azimuthal velocity at a fixed height $z = 1$ for various radial distances. In both plots, the velocity increases rapidly to a peak and then decays exponentially over time, capturing the characteristic intensification and subsequent weakening of the vortex. The peak velocity is highest near the core and diminishes as r increases, indicating that the strongest rotational effects are concentrated closer to the vortex centre.

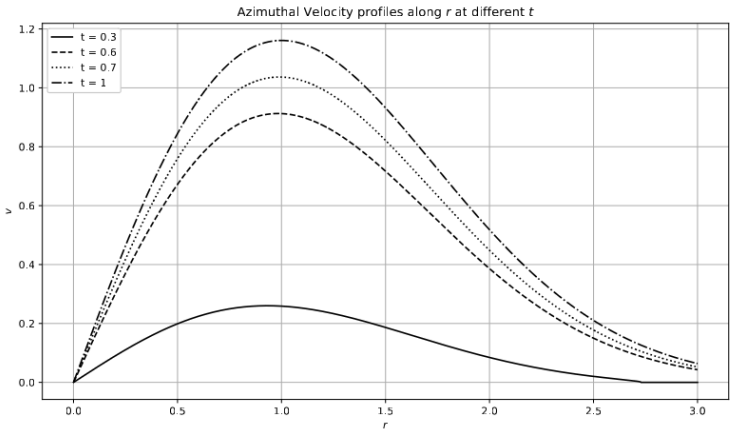

Figure 7.8: The plot presents the radial profiles of normalized azimuthal velocities for time range $0 - 1$ for $z = 1$, $\lambda = 2$, $Re = 1000$ and $A = 1$.

The role of the scaling factor λ in the formation dust devils is illustrated in Fig. (7.12). The plots are the radial profiles of azimuthal velocities corresponding to λ in the

range $0-2$. It is observed that azimuthal velocity decreases as λ increases, and ultimately the dust devil itself disappears as $\lambda \to \infty$. Contrary to that when $\lambda \to 0$.

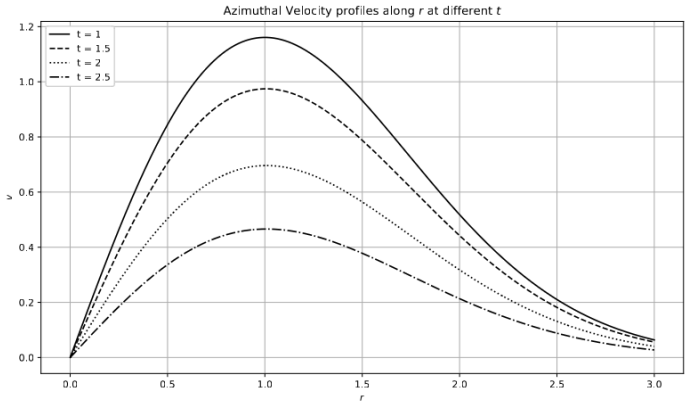

Figure 7.9: The plot presents the radial profiles of normalized azimuthal velocities for the time range $1 \leq t \leq 4$ at $z = 1$, with $\lambda = 2$, $Re = 1000$ and $A = 1$.

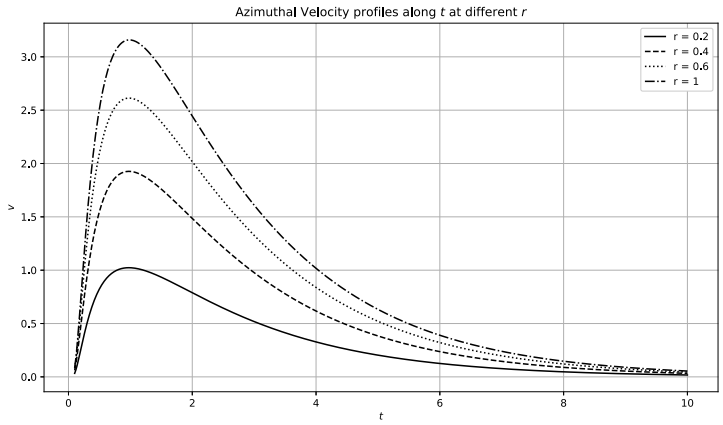

Figure 7.10: The plot presents the profiles of normalized azimuthal velocities over time for radii in the range $0 < r < 1$ at $z = 1$, with $\lambda = 1$ and $A = 1$.

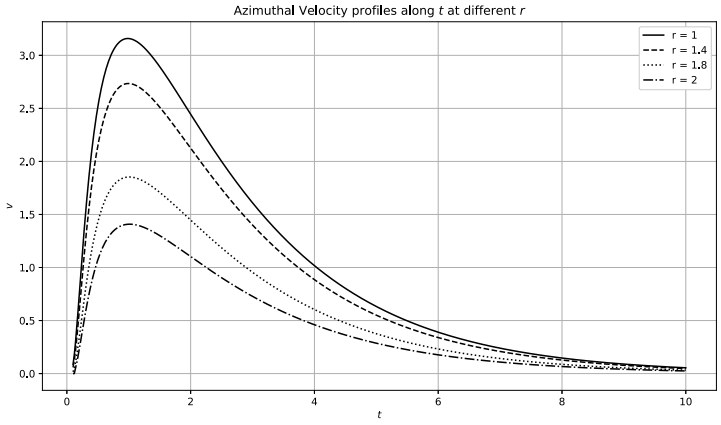

Figure 7.11: The plot presents the profiles of normalized azimuthal velocities over time for radii in the range $1 \leq r \leq 2$ at $z = 1$, with $\lambda = 1$ and $A = 1$.

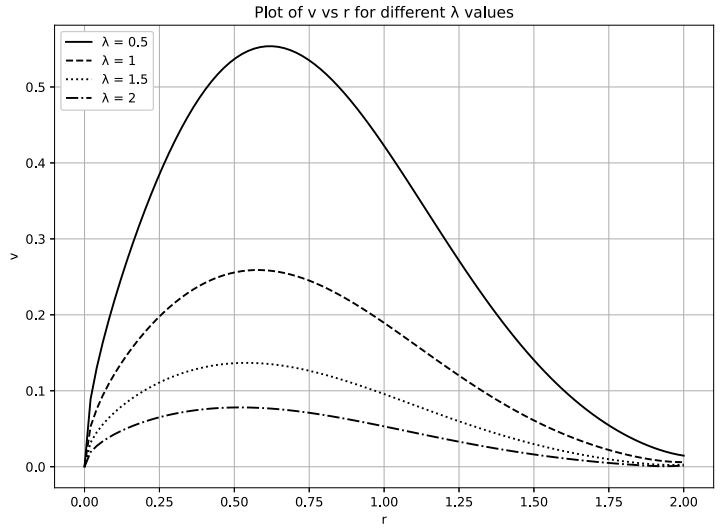

Figure 7.12: The plot presents the profiles of normalized azimuthal velocities over radius for different λ at $z = 1$, with $t = 1$ and $A = 1$.

7.3.4 Comparison with Observations

Property	Observation	Model Prediction
Maximum azimuthal velocity $v_{\max}$	10–30 m/s	$\sim$ 10–12 m/s
Core radius r_m	5–50 m	10 m (assumed)
Decay time (lifetime)	2–10 minutes	$\sim$ 200 seconds

Table 7.1: Comparison of model predictions with observed dust devil properties.

To assess the validity of the model, we compared its predictions with field observations of dust devils reported by Sinclair (1966) and Bluestein et al. (2004). For representative parameters ($r_m = 10\,\text{m}$, $v_m = 10\,\text{m/s}$), the model predicts a peak azimuthal velocity of approximately 10–12 m/s and a core radius of 10 m, both lying within the observed ranges (Table (7.1)). The estimated 200-second decay time is also consistent with the average lifetime of a dust devil. These comparisons imply that the model reasonably accurately depicts the main dynamical characteristics of dust devils.

7.3.5 Pressure Distribution Analysis

The main factor for the development of a dust devil is radial pressure distribution. Due to a substantial pressure difference between the axis and the outer boundary, dust devils occur in nature. Axial pressure gradient is deduced by substituting the derived radial and axial velocities from Eq. (7.11) into the z-momentum Eq. (7.8). Integration of the resulting equation gives pressure.

The radial pressure profiles for the time range $t \in [0, 1]$ and $t \in [1, 2]$ are shown in Fig. (7.13, 7.14) respectively. For the time evolution in Fig. (7.13) , where $t \in [0, 1]$, pressure is initially small at $t = 0.3$, suggesting the early formation phase of the dust

devil. As time progresses ($t = 0 - 1.0$), pressure deficit deepens, particularly near the centre ($r \approx 0$), which signifies the intensification of the dust devil.

Pressure remains low at $t = 1.0$, indicating that the dust devil is still in its mature phase with a strong central pressure deficit in $t \in [1, 2]$, observed in the Fig. (7.14). However, the pressure difference starts to decrease with time, especially at smaller radial distances r. With a slow recovery of pressure towards the centre, this pressure weakening shows that the dust devil is going through a decay phase. By $t = 2.0$ the central pressure has risen considerably, leading to dissipation of the vortex.

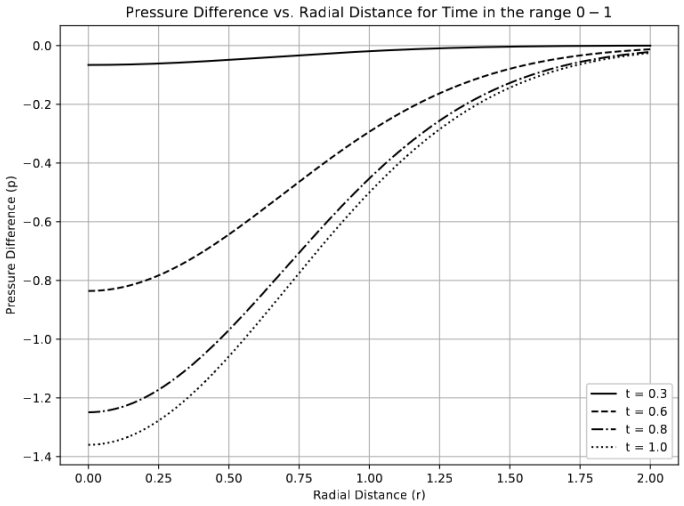

Figure 7.13: Radial profiles of pressure difference for time range $0-1$ at $z = 1$ for $\lambda = 1$ and $A = 1$.

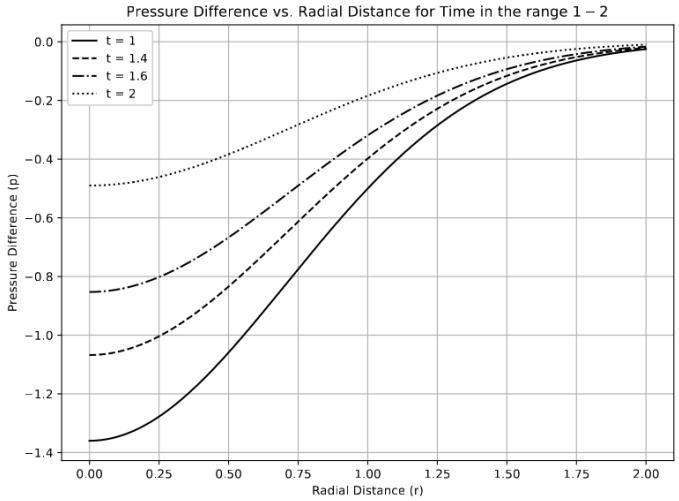

Figure 7.14: Radial profiles of pressure difference for time range $1-2$ at $z=1$ for $\lambda=1$ and $A=1$.

7.4 Conclusion

This study deals with the limitations of previous work that typically focused on either the genesis or the decay of the phenomenon. The model presents a time-dependent mathematical formulation for the entire life cycle of a dust devil. This model captures the evolution of radial, axial, and azimuthal velocities as well as the pressure distribution across spatial and temporal domains by using a stream function carefully chosen to best represent the dynamics of dust devils.

The radial velocity remains minimal near the vortex centre, increases to a maximum, and eventually diminishes outward. The radial velocity grows with time, reflecting the outward propagation of the radial flow of the vortex during the intensification phase ($t \in [0,1]$) while it decreases over time, indicating the gradual dissipation of the dust devil's radial motion during the decay phase ($t \in [1,2]$).

Similarly, the axial velocity shows the strong upward motion characteristic of dust devils. The axial velocity reaches its peak at the vortex centre, diminishing radially outward. In the intensification phase, this updraft strengthens, driven by surface heating. However, during the decay phase, the axial velocity weakens over time, reflecting the diminishing of vertical wind as the dust devil dissipates.

The azimuthal velocity exhibits the rotational dynamics of the dust devil, demonstrating a zero velocity at the vortex centre, a peak at an intermediate radius, and a decline at larger radial distances. During the growth phase, the azimuthal velocity increases with time, illustrating the strengthening of rotational forces as the dust devil intensifies. In the decay phase, the azimuthal velocity diminishes, highlighting the weakening of the vortex's rotational energy as the dust devil transitions toward equilibrium. The radial pressure profiles shows an increasing pressure with radius, highlighting the low-pressure centre of the dust devil. Dynamic pressure builds up as indicated by the exponential increase outward. When energy dissipates, the overall pressure difference gradually decreases, suggesting a weakening vortex. The dust devil's intensification and eventual gradual decay are reflected in this transition.

The main contribution of the study is its time-dependent approach to dust devil modelling. This work offers a unified formulation that captures the genesis, intensification, and decay of the dust devil, in contrast to earlier models that concentrated on particular life cycle stages. The findings provide fresh perspectives on the dissipation processes and temporal evolution of dust devils, in addition to being consistent with their known physical traits. The proposed framework's physical validity is further supported by a comparison of the model predictions and field observations of dust devils, which reveals good agreement in terms of decay timescales, core radius, and maximum azimuthal velocity.

Appendix A

Finding local minima and local maxima for u, taking constant $\lambda = 1$ for

$$u(r,t) = -Are^{-\lambda\frac{t^2+1}{t}}e^{-r^2} \tag{7.A.1}$$

We compute the first partial derivatives of $u(r,t)$:

$$\frac{\partial u}{\partial r} = -Ae^{-\lambda\frac{t^2+1}{t}}e^{-r^2}(1-2r^2),$$

$$\frac{\partial u}{\partial t} = A\lambda re^{-r^2}e^{-\lambda\frac{t^2+1}{t}}\left(1-\frac{1}{t^2}\right).$$

Critical points are found by solving $u_r = 0$ and $u_t = 0$. From $u_r = 0$:

$$-Ae^{-\lambda\frac{t^2+1}{t}}e^{-r^2}(1-2r^2) = 0. \tag{7.A.2}$$

This implies

$$r = \pm\frac{1}{\sqrt{2}}.$$

From $u_t = 0$:

$$A\lambda re^{-r^2}e^{-\lambda\frac{t^2+1}{t}}\left(1-\frac{1}{t^2}\right) = 0.$$

This implies

$$r = 0 \quad \text{or} \quad 1-\frac{1}{t^2} = 0 \quad \Rightarrow \quad t^2 = 1 \quad \Rightarrow \quad t = \pm 1. \tag{7.A.3}$$

The second-order partial derivatives are

$$u_{rr} = \frac{\partial^2 u}{\partial r^2} = 2Ar(3-2r^2)e^{-r^2-\lambda(t+\frac{1}{t})},$$

$$u_{tt} = \frac{\partial^2 u}{\partial t^2} = \frac{A\lambda^2 r\left(2t - (t^2-1)^2\right)}{t^4} e^{-r^2-\lambda(t+\frac{1}{t})},$$
$$u_{rt} = \frac{\partial^2 u}{\partial r \partial t} = \frac{2\lambda A r^2(1-t^2) + (t^2-1)}{t^2} e^{-r^2-\lambda(t+\frac{1}{t})}.$$

The discriminant of the Hessian matrix is given by

$$D = u_{rr}u_{tt} - (u_{rt})^2.$$

1. At $\left(\frac{1}{\sqrt{2}}, 1\right)$:

$$D = 4A^2e^{-5}, \quad u_{rr} = 2A^2\sqrt{2}e^{-5\lambda/2}.$$

   Since $D > 0$ and $u_{rr} > 0$, this is a **local minimum**.

2. At $\left(\frac{1}{\sqrt{2}}, -1\right)$:

$$D = -4A^2e^{3\lambda}.$$

   Since $D < 0$, this is a **saddle point**.

3. At $\left(-\frac{1}{\sqrt{2}}, 1\right)$:

$$D = 4A^2e^{-5}, \quad u_{rr} = -2A^2\sqrt{2}e^{-5/2}.$$

   Since $D > 0$ and $u_{rr} < 0$, this is a **local maximum**.

4. At $\left(-\frac{\sqrt{2}}{2}, -1\right)$:

$$D = -4A^2e^{3}.$$

   Since $D < 0$, this is a **saddle point**.

****

Overall conclusions and further scope of research

Overall conclusions

The phenomena discussed in this thesis are atmospheric vortices, specifically dust devils and tropical cyclones. The results explored are embodied in Chapters $3-7$.

Chapter 3 presents a significant advancement in the mathematical modelling of steady-state whirlwinds, with a particular focus on dust devils. This work builds upon the earlier model proposed by Vyas and Majdalani (2006), who assumed an azimuthal velocity of the form $v \propto \frac{1}{r}$. Their formulation has singularity at the vortex centre and fails to incorporate vertical coordinate dependence of azimuthal velocity. In contrast, the model developed in this chapter introduces a more realistic azimuthal velocity profile that depends explicitly on both the radial and axial coordinates. This new formulation remains finite at the centre of the vortex and is radially bounded, thereby addressing the key limitations of the earlier model. A significant modification in our formulation is the presence of a separability constant k, which is essential in determining the vortex strength. For regulating the intensity and dispersion of azimuthal velocity, this parameter enables the model to represent dust devils of different intensities. According to the analysis, the azimuthal velocity peaks close to $r = \frac{1}{\sqrt{2}}$ and then taper off smoothly in both directions, towards the vortex core and the outer borders. Additionally, the peak velocity moves closer to the vortex axis as k increases, suggesting a more concentrated rotating structure.

Chapter 4 presents an analytical model for tropical cyclones that incorporates viscous effects—marking a significant advancement over the inviscid framework of Cecil and Majdalani (2022). This model accounts for key physical features including vertical

wind structure, realistic boundary conditions, and cyclostrophic balance. The main objective is to understand how eye size influences cyclone intensity through its effect on radial, axial, and azimuthal velocities, as well as pressure distribution.

The flow is modelled for steady, incompressible, and axisymmetric, with physically consistent boundary conditions such as zero axial velocity at the surface and zero radial velocity at the vortex centre and beyond the eye-wall. The vertical velocity follows a sinusoidal form based on experimental insights, from which the remaining components are systematically derived. Pressure is obtained by integrating the axial momentum equation and applying cyclostrophic balance using the Vatistas profile at the surface.

A key contribution is the incorporation of the eye size parameter α and Reynolds number Re into the formulation. As α increases, azimuthal velocity peaks more sharply and falls rapidly in the rain-band, consistent with observational data. Larger eyes lead to more intense but localized rotational cores, while viscosity—quantified via Re—modulates the sharpness and distribution of velocity gradients. The pressure field increases radially outward from the eye, with steeper gradients for larger eyes and lower altitudes, highlighting the link between eye size, pressure drop, and storm intensity.

Chapter 5 presents a generalized analytical model for steady-state atmospheric vortices, incorporating viscous effects. Building upon the radial velocity structure proposed by Onishchenko et al. (2021), this work advances vortex modelling by deriving all three velocity components—radial, axial, and azimuthal—as functions of both radial and axial coordinates, ensuring they remain bounded throughout the domain. A key novelty of this model lies in its use of Rankine and Burgers velocity profiles as boundary conditions to enforce cyclostrophic balance at the ground level, thereby yielding a more realistic representation of vortex dynamics.

Unlike prior models that often assume unbounded or oversimplified velocity fields, the proposed framework introduces exponential localization in both the radial and vertical directions. The incorporation of physically consistent boundary conditions allows the model to capture the complete flow structure, including the converging radial inflow, central updraft, and rotational core, as observed in real atmospheric vortices. Furthermore, by varying the characteristic parameters such as the α and vortex sharpness parameter K, the model can represent a range of vortex intensities and morphologies—from dust devils to hurricanes.

Our analysis demonstrates that the azimuthal velocity exhibits distinct behaviour depending on the boundary condition employed. When Rankine's model is used, the velocity peaks sharply near the core and increases with height, whereas Burgers' condition results in smoother transitions and non-monotonic radial profiles. The model also reveals how radial pressure distributions vary with altitude and vortex size, providing insights into the mechanisms that drive vortex formation and intensification.

In Chapter 6 we present an analytical model for atmospheric vortices that incorporates all three velocity components—radial, axial, and azimuthal—along with a pressure field derived from the momentum equations. The model modifies the stream function to include a central low-pressure core and applies a viscous correction to the azimuthal velocity, enforcing the no-slip condition at the ground. Unlike classical models by Rankine, Burgers, or Vatistas, which assume infinite azimuthal velocity decay, our formulation confines rotational motion within a finite radial domain, capturing the compact structure of dust devils more realistically.

The model reveals height-dependent inflow-outflow transitions in radial velocity, strong near-surface axial updrafts that decay with height, and azimuthal velocity fields that peak near the core and weaken vertically. Parametric control via a shape factor and

Reynolds number allows for modelling a range of vortex intensities, from weak convective vortices to intense dust devils. Higher Reynolds numbers produce sharper, more localized velocity peaks, while variations in the low-pressure core size affect both strength and spread of the flow.

Chapter 7 introduces a time-dependent analytical model that covers the full life cycle of dust devils, from rapid formation to gradual decay. By incorporating time, this work extends beyond traditional steady-state models and provides a unified framework for analysing transient vortex behaviour. The model yields expressions for radial, axial and azimuthal velocities and pressure depending on time, offering better understanding of the mechanisms driving dust devil intensification and decay.

During the intensification phase ($t \in [0, 1]$), all three velocity components—radial, vertical, and azimuthal—increase with time, but each exhibits a distinct spatial pattern. The radial velocity, zero at the vortex centre, increases outward to a maximum near $r = 1/\sqrt{2}$ before declining beyond, reflecting the strengthening of inward flow. In contrast, the vertical velocity is maximum at the axis and decreases outward, representing a strong central updraft sustained by a low-pressure core. The azimuthal velocity, initially zero at the centre, rises with radius and peaks at $r = 1$ then starts to decrease.

As the vortex enters the decay phase ($t > 1$), all velocity components decrease gradually. The weakening starts at the periphery and moves inward, illustrating an outward-propagating dissipation. Interestingly, there is a continuous core circulation as the rotating component decays more slowly than the inflow. The vortex core maintains its maximum vertical velocity and zero radial velocity throughout its existence.

Future work

The analytical models developed in this thesis provide a foundational understanding of the dynamics of atmospheric vortices; however, there are still a number of unknown areas that may be investigated further. The consideration of thermodynamic effects, such as buoyancy, heat transfer, and latent heat release, which are crucial in the development and intensification of real-world vortices, particularly tropical cyclones, may be an interesting extension. By incorporating these aspects, models could become more physically complete and the current framework would be more applicable to climate research and weather forecasting.

Analytical modelling integrated with machine learning is an interesting and present-day trend for future research. Analytical models may be refined by means of data-driven approach by accounting fot complex patterns from observational data and high-resolution simulations that are difficult to capture analytically. For example, satellite data, reanalysis datasets, or Doppler radar observations can be used to train machine learning models to estimate model parameters like eddy viscosity or core size. Moreover, artificial models built using neural networks or Gaussian processes may rapidly approximate vortex activity for real-time forecasting and early warning systems. Hybrid modelling approaches —combining physical insight from analytical solutions with the adaptability of machine learning algorithms— are expected to be powerful in improving predictive capabilities. To explore genesis, intensification, and decay under different environmental conditions, for example, the time development of vortex properties could be modelled using temporal convolutional networks or recurrent neural networks. likewise unsupervised learning techniques might help in the classification of vortex type or the finding of hidden structures in huge datasets, improving our understanding of vortex classification and lifecycle patterns.

Combining mathematical models with machine learning enables more accurate forecasting, creating broader perspective in meteorology, climate science, and disaster preparedness.

****

Bibliography

Anthes, R. (2016). *Tropical cyclones: their evolution, structure and effects*, volume 19. Springer.

Anthes, R. A. (1966). Numerical modeling of tropical cyclone genesis. *Journal of the Atmospheric Sciences*, 23(6):745–758.

Aouaouda, M., Ayadi, A., and Yashima, H. F. (2019). Mathematical modeling of tropical cyclones on the basis of wind trajectories. *Computational Mathematics and Mathematical Physics*, 59:1493–1507.

Baker, C. and Sterling, M. (2017). Modelling wind fields and debris flight in tornadoes. *Journal of Wind Engineering and Industrial Aerodynamics*, 168:312–321.

Balme, M. and Greeley, R. (2006a). Dust devils on earth and mars. *Reviews of Geophysics*, 44(3).

Balme, M. and Greeley, R. (2006b). Dust devils on earth and mars. *Reviews of Geophysics*, 44(3):RG3003.

Batchelor, G. (1964). Axial flow in trailing line vortices. *Journal of Fluid Mechanics*, 20(4):645–658.

Battan, L. J. (1958). Energy of a dust devil. *Journal of the Atmospheric Sciences*, 15(2):235–237.

Ben-Amots, N. (2016). Dynamics and thermodynamics of a tornado: Rotation effects. *Atmospheric research*, 178:320–328.

Bloor, M. I. G. and Ingham, D. B. (1987). The flow in industrial cyclones. *Journal of Fluid Mechanics*, 178:507–519.

Bluestein, H. B. (2005). A review of ground-based, mobile, w-band doppler-radar observations of tornadoes and dust devils. *Dynamics of atmospheres and oceans*, 40(3):163–188.

Bluestein, H. B., Ladue, J. G., Stein, H., Speheger, D., and Unruh, W. F. (1993). Doppler radar wind spectra of supercell tornadoes. *Monthly weather review*, 121(8):2200–2222.

Bluestein, H. B., Lee, W.-C., Bell, M., Weiss, C. C., and Pazmany, A. L. (2003). Mobile doppler radar observations of a tornado in a supercell near bassett, nebraska, on 5 june 1999. part ii: Tornado-vortex structure. *Monthly weather review*, 131(12):2968–2984.

Bluestein, H. B., Weiss, C. C., and Pazmany, A. L. (2004). Doppler radar observations of dust devils in texas. *Monthly weather review*, 132(1):209–224.

Bretherton, F. and Turner, J. (1968). On the mixing of angular momentum in a stirred rotating fluid. *Journal of Fluid Mechanics*, 32(3):449–464.

Bryan, G. H. and Rotunno, R. (2009). Evaluation of an analytical model for the maximum intensity of tropical cyclones. *Journal of the Atmospheric Sciences*, 66(10):3042–3060.

Bryan, G. H. and Rotunno, R. (2010). The maximum intensity of tropical cyclones in axisymmetric numerical models. *Monthly Weather Review*, 138(4):1269–1285.

Burgers, J. M. (1948). A mathematical model illustrating the theory of turbulence. *Advances in applied mechanics*, 1:171–199.

Camp, J. P. and Montgomery, M. T. (2000). Hurricane maximum intensity: Past and present. *Monthly Weather Review*, 128(9):3235–3243.

Cantor, B. A., Kanak, K. M., and Edgett, K. S. (2006). Mars orbiter camera observations of martian dust devils and their tracks (september 1997 to january 2006) and evaluation of theoretical vortex models. *Journal of Geophysical Research: Planets*, 111(E12).

Carrier, G. F. (1975). On the intensification of hurricanes. *Journal of Fluid Mechanics*, 69(4):753–766.

Cecil, O. M. and Majdalani, J. (2022). On the generalized beltramian motion of the bidirectional vortex in a right-cylindrical cyclone with a hollow core. *Physics of Fluids*, 34(4):043603.

Chavas, D. R., Reed, K. A., and Knaff, J. A. (2017). Physical understanding of the tropical cyclone wind-pressure relationship. *Nature communications*, 8(1):1360.

Chen, X. and Zhang, F. (2023). A unified framework for tropical cyclone intensification and structure evolution in numerical models. *Journal of Advances in Modeling Earth Systems*, 15(2):e2022MS003456.

Church, C. and Snow, J. (1979). The dynamics of natural tornadoes as inferred from laboratory simulations. *J. Rech. Atmosph.*, 13(2):111–133.

Cohen, Y., Durden, S. L., Harnik, N., and Heifetz, E. (2019). Relating observations of gradient nonbalance at the top of hurricanes with their warm core structures. *Geophysical Research Letters*, 46(20):11510–11519.

Cohen, Y., Harnik, N., Heifetz, E., Nolan, D. S., Tao, D., and Zhang, F. (2017). On the violation of gradient wind balance at the top of tropical cyclones. *Geophysical Research Letters*, 44(15):8017–8026.

Cortese, T. and Balachandar, S. (1993). Vortical nature of thermal plumes in turbulent convection. *Physics of Fluids A: Fluid Dynamics*, 5(12):3226–3232.

Cronin, T. W. (2023). An analytic model for tropical cyclone outer winds. *Geophysical Research Letters*, 50(11):e2023GL103942.

Culick, F. (1966). Rotational axisymmetric mean flow and damping of acoustic waves in asolid propellant rocket. *AIAA Journal*, 4(8):1462–1464.

Davies-Jones, R. (1995). Tornadoes. *Scientific American*, 273:48.

Davies-Jones, R. (2015). A review of supercell and tornado dynamics. *Atmospheric Research*, 158:274–291.

Davies-Jones, R., Trapp, R. J., and Bluestein, H. B. (2001). Tornadoes and tornadic storms. In *Severe convective storms*, pages 167–221. Springer.

Davies-Jones, R. P. and Wood, V. T. (2006). Simulated doppler velocity signatures of evolving tornado-like vortices. *Journal of Atmospheric and Oceanic Technology*, 23(8):1029–1048.

Dawson, D. T. and Marquis, J. N. (2020). Tornadoes in supercell storms: Advances in observational, theoretical, and numerical modeling perspectives. *Journal of the Atmospheric Sciences*, 77(3):657–677.

DeMaria, M. and Kaplan, J. (1993). Sea surface temperature and the maximum intensity of atlantic tropical cyclones. *Journal of Climate*, 7(9):1324–1334.

Doyle, J. D., Moskaitis, J. R., Feldmeier, J. W., Ferek, R. J., Beaubien, M., Bell, M. M., Cecil, D. L., Creasey, R. L., Duran, P., Elsberry, R. L., et al. (2017). A view of tropical cyclones from above: The tropical cyclone intensity experiment. *Bulletin of the American Meteorological Society*, 98(10):2113–2134.

Duran, P. and Molinari, J. (2018). Dramatic inner-core tropopause variability during the rapid intensification of hurricane patricia (2015). *Monthly Weather Review*, 146(1):119–134.

Eliassen, A. (1951). Slow thermally or frictionally controlled meridional circulation in a circular vortex. *Astrophisica Norvegica, v. 5, p. 19*, 5:19.

Ellehoj, M. D., Gunnlaugsson, H. P., Taylor, P. A., Kahanpää, H., Bean, K. M., Cantor, B. A., Daerden, F., Drube, L., Fisher, D., Harri, A.-M., Holstein-Rathlou, C., Lange, C. F., Lemmon, M. T., Madsen, M. B., Malin, M. C., Polkko, J., Smith, P. H., Tamppari, L. K., and Woetzel, J. (2010). Convective vortices and dust devils at the phoenix mars mission landing site. *Journal of Geophysical Research: Planets*, 115:E00E16.

Elsaesser, D., Fedorowicz, K., and Utyuzhnikov, S. (2018). Towards the development of analytical tornado-like models. *AIP Advances*, 8(12).

Emanuel, K. (2003). Tropical cyclones. *Annual review of earth and planetary sciences*, 31(1):75–104.

Emanuel, K. (2005). *Divine wind: the history and science of hurricanes*. Oxford university press.

Emanuel, K. and Rotunno, R. (2011). Self-stratification of tropical cyclone outflow. part i: Implications for storm structure. *Journal of the Atmospheric Sciences*, 68(10):2236–2249.

Emanuel, K. A. (1986). An air-sea interaction theory for tropical cyclones. part i: Steady-state maintenance. *Journal of Atmospheric Sciences*, 43(6):585–605.

Emanuel, K. A. (1997). Some aspects of hurricane inner-core dynamics and energetics. *Journal of the Atmospheric Sciences*, 54(8):1014–1026.

Farrell, W., Delory, G., Cummer, S., and Marshall, J. (2003a). A simple electrodynamic model of a dust devil. *Geophysical Research Letters*, 30(20).

Farrell, W., Delory, G., Cummer, S., and Marshall, J. (2003b). A simple electrodynamic model of a dust devil. *Geophysical Research Letters*, 30(20).

Farrell, W., Renno, N., Delory, G., et al. (2006). Integration of electrostatic and fluid dynamics within a dust devil. *Journal of Geophysical Research: Planets*, 111(E1).

Farrell, W., Smith, P., Delory, G., et al. (2004). Electric and magnetic signatures of dust devils from the 2000–2001 matador desert test. *Journal of Geophysical Research: Planets*, 109(E3).

Farrell, W. M., Delory, G. T., Cummer, S. A., and Marshall, J. R. (2003c). A simple electrodynamic model of a dust devil. *Geophysical research letters*, 30(20).

Fenton, L. K. and Lorenz, R. (2015). Dust devil height and spacing with relation to the martian planetary boundary layer thickness. *Icarus*, 260:246–262.

Fernández, W. (1997). Martian dust storms: A review. *Earth, Moon, and Planets*, 77:19–46.

Ferrel, W. (1889). *Recent Advances in Meteorology*. Government Printing Office, Washington, D.C.

Fiedler, B. H. and Rotunno, R. (1986). A theory for the maximum windspeeds in tornado-like vortices. *Journal of the Atmospheric Sciences*, 43(21):2328–2340.

Fisher, J. A., Richardson, M. I., Newman, C. E., Szwast, M. A., Graf, C., Basu, S., Ewald, S. P., Toigo, A. D., and Wilson, R. J. (2005). A survey of martian dust devil activity using mars global surveyor mars orbiter camera images. *Journal of Geophysical Research: Planets*, 110(E3).

Franzese, G., Silvestro, S., Vaz, D. A., Popa, C. I., Cozzolino, F., Esposito, F., Mongelluzzo, G., Porto, C., and Ruggeri, A. C. (2021). Dust devils: Characteristics of the forward motion from a saharan survey. *Aeolian Research*, 50:100678.

Giersch, S. and Raasch, S. (2023). How do dust devil-like vortices depend on model resolution? a grid convergence study using large-eddy simulation. *Boundary-Layer Meteorology*, 187(3):703–742.

Gillmeier, S., Sterling, M., Baker, C., and Hemida, H. (2017). An analysis of non-stationary processes in tornado-like vortices. In *Physmod 2017 – International Workshop on Physical Modelling of Flow and Dispersion Phenomena*, page N/A, Birmingham, UK. Department of Civil Engineering, University of Birmingham. Presented at the Dynamics of Urban and Coastal Atmosphere – LHEEA, École Centrale de Nantes, France, 23–25 August 2017.

Gillmeier, S., Sterling, M., and Hemida, H. (2016). An analysis of the influence of a tornado generator's geometry on the flow field. In *Proceedings of the 8th International Colloquium on Bluff Body Aerodynamics and Applications*, page N/A, Boston, MA.

Gillmeier, S., Sterling, M., Hemida, H., and Baker, C. J. (2018). A reflection on analytical tornado-like vortex flow field models. *Journal of Wind Engineering and Industrial Aerodynamics*, 174:10–27.

Gray, W. M. (1979). Hurricanes: Their formation, structure and likely role in the tropical circulation. meteorology over the tropical oceans. *Roy. Meteor. Soc.*, pages 155–218.

Greeley, R., Balme, M. R., Iversen, J. D., Metzger, S., Mickelson, R., Phoreman, J., and White, B. (2003). Martian dust devils: Laboratory simulations of particle threshold. *Journal of Geophysical Research: Planets*, 108(E5).

Haan Jr, F. L., Sarkar, P. P., and Gallus, W. A. (2008). Design, construction and performance of a large tornado simulator for wind engineering applications. *Engineering Structures*, 30(4):1146–1159.

Harrison, R. G., Barth, E., Esposito, F., Merrison, J., Montmessin, F., Aplin, K. L., Borlina, C., Berthelier, J.-J., Déprez, G., Farrell, W. M., et al. (2016). Applications of electrified dust and dust devil electrodynamics to martian atmospheric electricity. *Space Science Reviews*, 203:299–345.

Heng, J. and Wang, Y. (2017). Nonlinear response of a tropical cyclone vortex to imposed sea surface temperature anomalies. *Journal of Climate*, 30(10):3563–3582.

Hess, G. and Spillane, K. (1990). Characteristics of dust devils in australia. *Journal of Applied Meteorology and Climatology*, 29(6):498–507.

Horn, S. and Aurnou, J. M. (2021). Tornado-like vortices in the quasi-cyclostrophic regime of coriolis-centrifugal convection. *Journal of Turbulence*, 22(4-5):297–324.

Horton, W., Miura, H., Onishchenko, O., Couedel, L., Arnas, C., Escarguel, A., Benkadda, S., and Fedun, V. (2016). Dust devil dynamics. *Journal of Geophysical Research: Atmospheres*, 121(12):7197–7214.

Hueso, R., Newman, C., del Río-Gaztelurrutia, T., Munguira, A., Sánchez-Lavega, A., Toledo, D., Apéstigue, V., Arruego, I., Vicente-Retortillo, A., Martínez, G., et al. (2023). Convective vortices and dust devils detected and characterized by mars 2020. *Journal of Geophysical Research: Planets*, 128(2):e2022JE007516.

Ito, J. and Niino, H. (2014). Particle image velocimetry of a dust devil observed in a desert. *SOLA*, 10:108–111.

Izvekova, Y. N. and Popel, S. (2016). Charged dust motion in dust devils on earth and mars. *Contributions to Plasma Physics*, 56(3-4):263–269.

Izvekova, Y. N. and Popel, S. (2017). Plasma effects in dust devils near the martian surface. *Plasma Physics Reports*, 43:1172–1178.

Izvekova, Y. N. and Popel, S. (2020). Electric field influence on dust particle dynamics in dust vortices. In *Journal of Physics: Conference Series*, volume 1556, page 012071. IOP Publishing.

Jackson, B., Lorenz, R. D., and Balme, M. (2020). Dust devil population statistics from field observations spanning 5 decades. *Journal of Geophysical Research: Atmospheres*, 125(6):e2019JD032185.

Kahanpää, H. and Viúdez-Moreiras, D. (2021). Modelling martian dust devils using in-situ wind, pressure, and uv radiation measurements by mars science laboratory. *Icarus*, 359:114207.

Kanak, K. M. (2005). Numerical simulation of dust devil-scale vortices. *Quarterly Journal of the Royal Meteorological Society: A journal of the atmospheric sciences, applied meteorology and physical oceanography*, 131(607):1271–1292.

Kanak, K. M., Lilly, D. K., and Snow, J. T. (2000). The formation of vertical vortices in the convective boundary layer. *Quarterly Journal of the Royal Meteorological Society*, 126(569):2789–2810.

Kepert, J. (2001). The dynamics of boundary layer jets within the tropical cyclone core. part i: Linear theory. *Journal of the Atmospheric Sciences*, 58(17):2469–2484.

Kieu, C. Q. (2012). An investigation into the contraction of the hurricane radius of maximum wind. *Meteorology and Atmospheric Physics*, 115(1-2):47–56.

Kieu, C. Q. and Zhang, D.-L. (2009). An analytical model for the rapid intensification of tropical cyclones. *Quarterly Journal of the Royal Meteorological Society: A journal of the atmospheric sciences, applied meteorology and physical oceanography*, 135(642):1336–1349.

Kim, Y. C. and Matsui, M. (2017). Analytical and empirical models of tornado vortices: A comparative study. *Journal of Wind Engineering and Industrial Aerodynamics*, 171:230–247.

Kolomenskiy, D. and Moffatt, H. (2012). Similarity solutions for unsteady stagnation point flow. *Journal of Fluid Mechanics*, 711:394–410.

Kosiba, K. A., Trapp, R. J., and Wurman, J. (2008). An analysis of the axisymmetric three-dimensional low level wind field in a tornado using mobile radar observations. *Geophysical Research Letters*, 35(5).

Kossin, J. P. and Schubert, W. H. (2001). Mesovortices, polygonal flow patterns, and rapid pressure falls in hurricane-like vortices. *Journal of the atmospheric sciences*, 58(15):2196–2209.

Kuo, H. (1971). Axisymmetric flows in the boundary layer of a maintained vortex. *Journal of the Atmospheric sciences*, 28(1):20–41.

Kurgansky, M. V. (2022). Statistical distribution of atmospheric dust devils on earth and mars. *Boundary-Layer Meteorology*, 184(3):381–400.

Kurihara, Y. and Tuleya, R. E. (1974). Structure of a tropical cyclone developed in a three-dimensional numerical simulation model. *Journal of Atmospheric Sciences*, 31(4):893–919.

Lamb, H. (1932). *Hydrodynamics*. Cambridge University Press, Cambridge, 6th edition.

Larcheveque, M. and Chaskalovic, J. (1994). A new mathematical model applied to tornado genesis. *International journal of engineering science*, 32(1):187–193.

Lee, J. (2004). Pressure measurements at the ground in an f-4 tornado. p 15.3. In *Extended Abstract of 22nd Conf. on Severe Local Storms, Hyannis, MA, 4-8 October 2004, Amer. Meteor. Soc.*

Lee, W.-C. and Wurman, J. (2005). Diagnosed three-dimensional axisymmetric structure of the mulhall tornado on 3 may 1999. *Journal of the atmospheric sciences*, 62(7):2373–2393.

Lewellen, D., Lewellen, W., and Xia, J. (2000). The influence of a local swirl ratio on tornado intensification near the surface. *Journal of the atmospheric sciences*, 57(4):527–544.

Lewellen, W. (1993). Tornado vortex theory. *Geophysical Monograph Series*, 79:19–39.

Lewellen, W., Lewellen, D., and Sykes, R. (1997). Large-eddy simulation of a tornado's interaction with the surface. *Journal of the atmospheric sciences*, 54(5):581–605.

Li, Q. and Wang, Y. (2019). A comparison of inner-core structure in tropical cyclones simulated with different model resolutions. *Monthly Weather Review*, 147(8):2797–2818.

Li, Y., Wang, Y., and Lin, Y. (2019). Revisiting the dynamics of eyewall contraction of tropical cyclones. *Journal of the Atmospheric Sciences*, 76(10):3229–3245.

Liu, Z. and Ishihara, T. (2016). and industrial aerodynamics. *J. Wind Eng. Ind. Aerodyn*, 152:41–49.

Long, R. R. (1961). A vortex in an infinite viscous fluid. *Journal of Fluid Mechanics*, 11(4):611–624.

Majdalani, J. (2022). On the generalized beltramian motion of the bidirectional vortex in a conical cyclone. *Physics of Fluids*, 34(3).

Majdalani, J. and Chiaverini, M. J. (2002). On steady rotational cyclonic flows: The viscous bidirectional vortex. *Physics of Fluids*, 14(3):853–861.

Majdalani, J. and Chiaverini, M. J. (2009). On steady rotational cyclonic flows: The viscous bidirectional vortex. *Physics of Fluids*, 21(10).

Majumdar, K. K. (2003). A mathematical model of the nascent cyclone. *IEEE transactions on geoscience and remote sensing*, 41(5):1118–1122.

Makarieva, A. M., Gorshkov, V. G., and Nefiodov, A. V. (2011). Condensational theory of stationary tornadoes. *Physics Letters A*, 375(24):2259–2261.

Malkus, J. S. and Riehl, H. (1960). On the dynamics and energy transformations in steady-state hurricanes. *Tellus*, 12(1):1–20.

Malkus, J. S. and Riehl, H. (1998). On the dynamics and energy transformation in hurricanes. *Tellus, 50th Anniversary Collection*, 12(1):1–17. Reprint of 1960 article.

McGinnigle, J. (1966). Dust whirls in north-west libya. *Weather*, 21(8):272–276.

Melnik, O. and Parrot, M. (1998). Electrostatic discharge in martian dust storms. *Journal of Geophysical Research: Space Physics*, 103(A12):29107–29117.

Michaels, T. I. and Rafkin, S. C. (2004). Large-eddy simulation of atmospheric convection on mars. *Quarterly Journal of the Royal Meteorological Society*, 130(599):1251–1274.

Miller, B. I. (1958). On the maximum intensity of hurricanes. *Journal of Atmospheric Sciences*, 15(2):184–195.

Miyamoto, Y. and Takemi, T. (2015). A transition mechanism for the spontaneous axisymmetric intensification of tropical cyclones. *Journal of the Atmospheric Sciences*, 72(1):112–129.

Moffatt, H. (2000). The interaction of skewed vortex pairs: a model for blow-up of the navier–stokes equations. *Journal of Fluid Mechanics*, 409:51–68.

Montgomery, M. T., Sang, N. V., Smith, R. K., and Persing, J. (2009). Do tropical cyclones intensify by wishe? *Quarterly Journal of the Royal Meteorological Society: A journal of the atmospheric sciences, applied meteorology and physical oceanography*, 135(644):1697–1714.

Montgomery, M. T. and Smith, R. K. (2014). Paradigms for tropical cyclone intensification. *Australian Meteorological and Oceanographic Journal*, 64(1):37–66.

Natarajan, D. and Hangan, H. (2012). Large eddy simulations of translation and surface roughness effects on tornado-like vortices. *Journal of Wind Engineering and Industrial Aerodynamics*, 104:577–584.

Neakrase, L. D. and Greeley, R. (2010). Dust devils in the laboratory: Effect of surface roughness on vortex dynamics. *Journal of Geophysical Research: Planets*, 115(E5).

Nguyen, C. M., Reeder, M. J., and Davidson, N. E. (2003). A numerical study of tropical cyclone intensification. *Quarterly Journal of the Royal Meteorological Society*, 129(590):1841–1866.

Nolan, D. S. and Montgomery, M. T. (2012). Nonhydrostatic numerical simulations of tropical cyclones: Sensitivity to vortex structure. *Journal of the Atmospheric Sciences*, 69(7):2108–2127.

Nolan, D. S., Montgomery, M. T., and Grasso, L. D. (2001). The wavenumber-one instability and trochoidal motion of hurricane-like vortices. *Journal of the atmospheric sciences*, 58(21):3243–3270.

Nolan, D. S., Moon, Y., and Stern, D. P. (2007). Tropical cyclone intensification from asymmetric convection: Energetics and efficiency. *Journal of the Atmospheric Sciences*, 64(10):3377–3405.

Oke, A., Tapper, N. J., and Dunkerley, D. (2007). Willy-willies in the australian landscape: The role of key meteorological variables and surface conditions in defining frequency and spatial characteristics. *Journal of arid environments*, 71(2):201–215.

Onishchenko, O., Fedun, V., Ballai, I., Kryshtal, A., and Verth, G. (2021a). Generation of localised vertical streams in an unstable stratified atmosphere. *Fluids*, 6(12):454.

Onishchenko, O., Fedun, V., Horton, W., Pokhotelov, O., Astafieva, N., Skirvin, S., and Verth, G. (2021b). The stationary concentrated vortex model. climate 2021, 9, 39.

Onishchenko, O., Fedun, V., Horton, W., Pokhotelov, O., and Verth, G. (2019). Dust devils: Structural features, dynamics and climate impact. *Climate*, 7(1):12.

Onishchenko, O., Horton, W., Pokhotelov, O., and Stenflo, L. (2014a). Dust devil generation. *Physica Scripta*, 89(7):075606.

Onishchenko, O., Pokhotelov, O., and Astafieva, N. (2018). A novel model of quasi-stationary vortices in the earth's atmosphere. *Izvestiya, Atmospheric and Oceanic Physics*, 54:906–910.

Onishchenko, O., Pokhotelov, O., Horton, W., and Fedun, V. (2015). Dust devil vortex generation from convective cells. In *Annales Geophysicae*, volume 33, pages 1343–1347. Copernicus GmbH Göttingen, Germany.

Onishchenko, O., Pokhotelov, O., Horton, W., Smolyakov, A., Kaladze, T., and Fedun, V. (2014b). Rolls of the internal gravity waves in the earth's atmosphere. In *Proceedings of the Conference Name*, pages 181–186, Conference Location. Copernicus Publications, Copernicus Publications. Published in Annales Geophysicae.

Ooyama, K. (1969). Numerical simulation of the life cycle of tropical cyclones. *Journal of the Atmospheric Sciences*, 26(1):3–40.

Oseen, C. (1911). About vortex motion in a rubbing liquid, ark. *Foer Mat. Astron. Och Fys*.

Pandey, S. K. and Maurya, J. P. (2017). Exploration of characteristics governing dynamics of whirlwinds: application to dust devils. *Zeitschrift für Naturforschung A*, 72(8):763–778.

Pandey, S. K. and Maurya, J. P. (2018a). Exact solutions for unsteady axisymmetric vortex motions governing atmospheric vortices. *Dynamics of Atmospheres and Oceans*, 83:111–121.

Pandey, S. K. and Maurya, J. P. (2018b). A mathematical model governing tornado dynamics: An exact solution of a generalized model. *Zeitschrift für Naturforschung A*, 73(8):753–766.

Pandey, S. K. and Maurya, J. P. (2020). A general viscous model for some aspects of tropical cyclonic winds. *Zeitschrift für Naturforschung A*, 75(4):301–315.

Pandey, S. K. and Yadav, K. (2024). A mathematical model for viscous flow dynamics of tropical cyclones. *European Journal of Mechanics-B/Fluids*.

Peng, K., Rotunno, R., and Bryan, G. H. (2018). Evaluation of a time-dependent model for the intensification of tropical cyclones. *Journal of the Atmospheric Sciences*, 75(6):2125–2138.

Persing, J. and Montgomery, M. T. (2006). Is environmental cape important in the determination of maximum possible hurricane intensity? *Journal of the Atmospheric Sciences*, 63(12):3112–3127.

Rankine, W. (1882). A manual of applied physics. *Charles Griff and Co.: London, UK*.

Refan, M., Hangan, H., and Wurman, J. (2014). Reproducing tornadoes in laboratory using proper scaling. *Journal of Wind Engineering and Industrial Aerodynamics*, 135:136–148.

Refan, M., Hangan, H., Wurman, J., and Kosiba, K. (2017). Doppler radar-derived wind field of five tornado events with application to engineering simulations. *Engineering Structures*, 148:509–521.

Reiss, D., Spiga, A., and Erkeling, G. (2014). The horizontal motion of dust devils on mars derived from crism and ctx/hirise observations. *Icarus*, 227:8–20.

Rennó, N. O., Burkett, M. L., and Larkin, M. P. (1998). A simple thermodynamical theory for dust devils. *Journal of the atmospheric sciences*, 55(21):3244–3252.

Renno, N. O., Burkett, M. L., and Larkin, M. P. (1998). A simple thermodynamical theory for dust devils. *Journal of the Atmospheric Sciences*, 55(21):3244–3252.

Rogers, R. F., Reasor, P. D., Zawislak, J. A., and Nguyen, L. T. (2020). Precipitation processes and vortex alignment during the intensification of a weak tropical cyclone in moderate vertical shear. *Monthly Weather Review*, 148(5):1899–1929.

Rott, N. (1958). On the viscous core of a line vortex. *Zeitschrift für angewandte Mathematik und Physik ZAMP*, 9:543–553.

Rotunno, R. (2013). The fluid dynamics of tornadoes. *Annual review of fluid mechanics*, 45:59–84.

Rotunno, R. and Emanuel, K. A. (1987). An air–sea interaction theory for tropical cyclones. part ii: Evolutionary study using a nonhydrostatic axisymmetric numerical model. *Journal of Atmospheric Sciences*, 44(3):542–561.

Rotunno, R. and Emanuel, K. A. (1988). An air-sea interaction theory for tropical cyclones. part ii: Evolutionary structure. *Journal of the Atmospheric Sciences*, 45(3):525–547.

Ryan, J. and Carroll, J. (1970). Dust devil wind velocities: Mature state. *Journal of Geophysical Research*, 75(3):531–541.

Shapiro, A. and Kogan, Y. (1994). On vortex formation in multicell convective clouds in a shear-free environment. *Atmospheric research*, 33(1-4):125–136.

SHAPIRO, L. J. (1982). 1014 volume 110 monthly weather review. *Monthly Weather Review*, 110(20):1014.

Shapiro, L. J. (1982). Hurricane structure and energetics as simulated by a diagnostic model. *Journal of the Atmospheric Sciences*, 39(8):1749–1766.

Sheel, V., Uttam, S., and Mishra, S. (2021). Numerical simulation of dust lifting within a steady state dust devil. *Journal of Geophysical Research: Planets*, 126(11):e2021JE006835.

Sinclair, P. C. (1964). Some preliminary dust devil measurements. *Monthly Weather Review*, 92(8):363–367.

Sinclair, P. C. (1965). On the rotation of dust devils. *Bulletin of the American Meteorological Society*, 46(7):388–391.

Sinclair, P. C. (1966). A quantitative analysis of the dust devil.

Sinclair, P. C. (1969). General characteristics of dust devils. *Journal of Applied Meteorology*, 8(1):32–45.

Sinclair, P. C. (1973). The lower structure of dust devils. *Journal of the Atmospheric Sciences*, 30(8):1599–1619.

Smith, R. and Leslie, L. (1976). Thermally driven vortices: A numerical study with application to dust-devil dynamics. *Quarterly Journal of the Royal Meteorological Society*, 102(434):791–804.

Smith, R. K. (2006). Lectures on tropical cyclones.

Smith, R. K., Montgomery, M. T., and Persing, J. (2014). On steady-state tropical cyclones. *Quarterly Journal of the Royal Meteorological Society*, 140(685):2638–2649.

Snow, J. T. and McClelland, T. M. (1990). Dust devils at white sands missile range, new mexico: 1. temporal and spatial distributions. *Journal of Geophysical Research: Atmospheres*, 95(D9):13707–13721.

Sohn, S.-I. (2020). An inviscid model of unsteady separated vortical flow for a moving plate. *Theoretical and Computational Fluid Dynamics*, 34(3):187–213.

Stern, D. P., Vigh, J. L., Nolan, D. S., and Zhang, F. (2015). Revisiting the relationship between eyewall contraction and intensification. *Journal of the Atmospheric Sciences*, 72(4):1283–1306.

Stull, R. B. (2015). *Practical meteorology: an algebra-based survey of atmospheric science*. University of British Columbia.

Sullivan, R. D. (1959). A two-cell vortex solution of the navier-stokes equations. *Journal of the Aerospace Sciences*, 26(11):767–768.

Tang, Z., Feng, C., Wu, L., Zuo, D., and James, D. L. (2018). Characteristics of tornado-like vortices simulated in a large-scale ward-type simulator. *Boundary-layer meteorology*, 166:327–350.

Taylor, G. I. (1918). Phenomena connected with turbulence in the lower atmosphere. *Proceedings of the Royal Society of London. Series A, Containing Papers of a Mathematical and Physical Character*, 94(658):137–155.

Toigo, A., Richardson, M., Ewald, S., and Gierasch, P. (2003). Numerical simulation of martian dust devils. *Journal of Geophysical Research: Planets*, 108(E6).

Vatistas, G., Lin, S., and Kwok, C. (1986). Theoretical and experimental studies on vortex chamber flows. *AIAA journal*, 24(4):635–642.

Vatistas, G. H., Kozel, V., and Mih, W. (1991). A simpler model for concentrated vortices. *Experiments in Fluids*, 11:73–76.

Vyas, A., Majdalani, J., and Chiaverini, M. (2003). The bidirectional vortex. part 2: viscous core corrections. In *39th AIAA/ASME/SAE/ASEE joint propulsion conference and exhibit*, page 5053.

Vyas, A. B. and Majdalani, J. (2006). Exact solution of the bidirectional vortex. *AIAA journal*, 44(10):2208–2216.

Vyas, A. B. and Majdalani, J. (2007). The bidirectional vortex. part 2: Viscous core corrections. *Journal of Fluid Mechanics*, 583:173–188.

Wakimoto, R. M. and Wilson, J. W. (1989). Non-supercell tornadoes. *Monthly Weather Review*, 117(6):1113–1140.

Ward, N. B. (1972). The exploration of certain features of tornado dynamics using a laboratory model. *Journal of Atmospheric Sciences*, 29(6):1194–1204.

Willis, G. and Deardorff, J. (1979). Laboratory observations of turbulent penetrative-convection planforms. *Journal of Geophysical Research: Oceans*, 84(C1):295–302.

Willoughby, H. (1979). Forced secondary circulations in hurricanes. *Journal of Geophysical Research: Oceans*, 84(C6):3173–3183.

Willoughby, H. (1990a). Temporal changes of the primary circulation in tropical cyclones. *Journal of Atmospheric Sciences*, 47(2):242–264.

Willoughby, H. and Rahn, M. (2004). Parametric representation of the primary hurricane vortex. part i: Observations and evaluation of the holland (1980) model. *Monthly Weather Review*, 132(12):3033–3048.

Willoughby, H. E. (1990b). Gradient balance in tropical cyclones. *Journal of the Atmospheric Sciences*, 47(2):265–274.

Wood, V. T. and Brown, R. A. (2011). Simulated tornadic vortex signatures of tornado-like vortices having one-and two-celled structures. *Journal of applied meteorology and climatology*, 50(11):2338–2342.

Wood, V. T. and White, L. W. (2011). A new parametric model of vortex tangential-wind profiles: Development, testing, and verification. *Journal of the Atmospheric Sciences*, 68(5):990–1006.

Wood, V. T., White, L. W., Willoughby, H. E., and Jorgensen, D. P. (2013). A new parametric tropical cyclone tangential wind profile model. *Monthly weather review*, 141(6):1884–1909.

Wu, Y., Chen, Q., and Li, M. (2024). A hybrid modeling approach for simulating tornado-induced wind fields using physics and machine learning. *Atmospheric Research*, 290:106933.

Wurman, J., Straka, J. M., and Rasmussen, E. N. (1996). Fine-scale doppler radar observations of tornadoes. *Science*, 272(5269):1774–1777.

Xiang, R. and Lee, K. (2005). Numerical study of flow field in cyclones of different height. *Chemical Engineering and Processing: Process Intensification*, 44(8):877–883.

Xie, L., Ling, Y., and Zheng, X. (2007). Laboratory measurement of saltating sand particles' angular velocities and simulation of its effect on saltation trajectory. *Journal of Geophysical Research: Atmospheres*, 112(D12).

Xu, J. and Wang, Y. (2020). Sensitivity of tropical cyclone intensification to inner-core structure. *Journal of the Atmospheric Sciences*, 77(4):1413–1432.

Xu, Z. and Hangan, H. (2009). An inviscid solution for modeling of tornadolike vortices. *J. Appl. Mech.*, 76(3):031011.

Yadav, K., Maurya, J. P., and Pandey, S. K. (2024). A generalized analytical viscous model for steady-state atmospheric vortices. *Physica Scripta*, 99(7):075233.

Ying, S. J. and Chang, C. (1970). Exploratory model study of tornado-like vortex dynamics. *Journal of Atmospheric Sciences*, 27(1):3–14.

Zhang, H., Wang, H., Xu, Z., and Khoo, B. C. (2023). A novel three-dimensional analytical tornado model constructed based on force balance analysis. *Physics of Fluids*, 35(6).

Zhao, Y., Gu, Z., Yu, Y., Ge, Y., Li, Y., and Feng, X. (2004). Mechanism and large eddy simulation of dust devils. *Atmosphere-Ocean*, 42(1):61–84.

Zheng, X., Huang, N., and Zhou, Y. (2003). Laboratory measurement of electrification of wind-blown sands and simulation of its effect on sand saltation movement. *Journal of Geophysical Research: Atmospheres*, 108(D10).

Zhou, L., Smith, T. M., and Gagne, D. J. (2022). Deep learning for tornado prediction using environmental and radar data. *Weather and Forecasting*, 37(1):1–18.

Zhou, Y., Guo, X., and Zheng, X. (2002). Experimental measurement of wind-sand flux and sand transport for naturally mixed sands. *Physical Review E*, 66(2):021305.

List of Publications

1. **Kriti Yadav**, Jagdish Prasad Maurya, and Sanjay Kumar Pandey, ”A generalized analytical viscous model for steady-state atmospheric vortices,” **Physica Scripta**, **99**(7), (2024) 075233.

2. Sanjay Kumar Pandey and **Kriti Yadav**, ”A mathematical model for viscous flow dynamics of tropical cyclones,” **European Journal of Mechanics - B/Fluids**, **111**, (2025) 72–80.

3. Sanjay Kumar Pandey and **Kriti Yadav**, ”A temporal model for the complete life-cycle of dust devils: From genesis to decay,” (Under Review).

4. Sanjay Kumar Pandey and **Kriti Yadav**, ”A viscous model for atmospheric vortices with a central depression of pressure,” (Under Review)

5. Sanjay Kumar Pandey and **Kriti Yadav**, ”An analytical model for whirlwinds of finite width rising with bounded velocity and decaying outflow: Application to dust devils,” (Communicated)

6. Sanjay Kumar Pandey and **Kriti Yadav**,” An Analysis of Generalized Velocity Field for Atmospheric Vortices: Application to Dust Devils” (Communicated).

****